ADVANCED MATERIALS
www.advmat.de

Understanding and Suppressing Non-Radiative Recombination Losses in Non-Fullerene Organic Solar Cells

Quan Liu and Koen Vandewal**

Organic solar cells benefit from non-fullerene acceptors (NFA) due to their high absorption coefficients, tunable frontier energy levels, and optical gaps, as well as their relatively high luminescence quantum efficiencies as compared to fullerenes. Those merits result in high yields of charge generation at a low or negligible energetic offset at the donor/NFA heterojunction, with efficiencies over 19% achieved for single-junction devices. Pushing this value significantly over 20% requires an increase in open-circuit voltage, which is currently still well below the thermodynamic limit. This can only be achieved by reducing non-radiative recombination, and hereby increasing the electroluminescence quantum efficiency of the photo-active layer. Here, current understanding of the origin of non-radiative decay, as well as an accurate quantification of the associated voltage losses are summarized. Promising strategies for suppressing these losses are highlighted, with focus on new material design, optimization of donor–acceptor combination, and blend morphology. This review aims at guiding researchers in their quest to find future solar harvesting donor–acceptor blends, which combine a high yield of exciton dissociation with a high yield of radiative free carrier recombination and low voltage losses, hereby closing the efficiency gap with inorganic and perovskite photovoltaics.

1. Introduction

The use of fullerene derivatives, especially [6,6]-Phenyl-C71-butyric acid methyl ester ($PC_{71}BM$), as electron acceptors has been crucial for the development of organic solar cells (OSC) enabling efficiencies of up to 12% in 2016.[1,2] While having appropriate charge transport properties, fullerenes are generally weakly absorbing. Most of the sunlight is therefore absorbed by the donor material, often a conjugated polymer, which in a blend with the acceptor forms a bulk heterojunction (BHJ) photo-active layer. For a large set of polymer: fullerene BHJs, the charge generation yield reaches a maximum when ≈0.4-0.8 eV of energy is lost per photon in the exciton dissociation process.[3–7] This energy loss, given by the energetic offset between the lowest singlet (S_1) and charge-transfer (CT) states, $\Delta E_{S1,CT}$, is thus substantial in the most efficient fullerene-based solar cells. The currently highest efficiency, Y-series of non-fullerene acceptors (NFA), however, enables OSCs with high external quantum efficiencies (EQE_{PV}) and fill factors (*FF*) at a marginal $\Delta E_{S1,CT}$.[8–11] NFAs benefit from a combination of good charge transport properties, optimized film morphologies, as well as high absorption coefficients, up to 1.5×10^5 cm^{-1} (compared to 1.0–5.0×10^4 cm^{-1} for fullerenes) in the visible and near-infrared.[8,12–14] An additional and significant advantage in the optimization of the photovoltaic properties of donor: NFA blends are their relatively straightforward adjustment of the frontier energy levels and optical gaps over a wide energy range, by engineering acceptor–donor–acceptor (A–D–A) or A–DA'D–A-type (such as Y6) fused groups in their molecular backbones.[15–18] This has brought the power conversion efficiency (*PCE*) of the state-of-the-art NFA OSCs to over 19% in a single-junction[19–25] and 20% in a two-terminal tandem configuration,[26,27] respectively.

Despite this great progress, organic solar cells still lag that of crystalline silicon (*c*-Si), copper indium gallium selenide (CIGS) and gallium arsenide (GaAs), as well as the emerging lead-halide inorganic–organic hybrid perovskites. **Figure 1**a compares photovoltaic parameters for these technologies. The optical gap of the highest efficiency NFA-based device so far is ≈1.4 eV which is comparable to that of GaAs. Both the short-circuit photocurrent (J_{SC}) and *FF* of the best OSC are within ≈10% of those of GaAs. However, the V_{oc} (0.89 V) is 20% lower than that of GaAs (1.12 V). Increasing the power conversion efficiency of OSCs to values comparable to inorganic solar cells thus requires simultaneously improving light absorption and charge transport properties for improved photocurrents and *FF*s while decreasing voltage losses. The latter is defined as the difference between the

Q. Liu, K. Vandewal
Hasselt University
IMOMEC
Wetenschapspark 1, Diepenbeek 3590, Belgium
E-mail: liuquan@nimte.ac.cn; koen.vandewal@uhasselt.be
Q. Liu
Zhejiang Provincial Engineering Research Center of Energy Optoelectronic Materials and Devices
Ningbo Institute of Materials Technology and Engineering
Chinese Academy of Sciences
Ningbo 315201, China

The ORCID identification number(s) for the author(s) of this article can be found under https://doi.org/10.1002/adma.202302452

DOI: 10.1002/adma.202302452

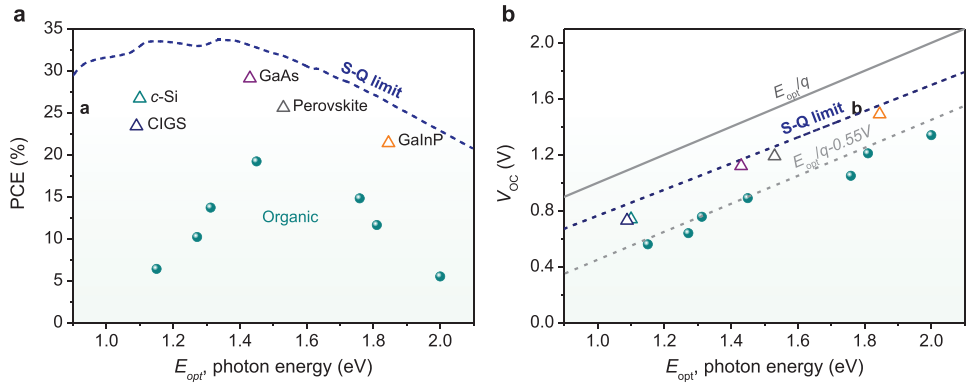

Figure 1. A comparison between state-of-the-art organic solar cells (OSCs) with inorganic and perovskite technologies. a) Plot of the power conversion efficiency (PCE) as a function of optical gap energy (E_{opt}) for single-junction solar cells. Triangles present the record PCEs for different types of inorganic or perovskite photovoltaic materials. Blue dots present a series of selected best-performing OSCs with various optical gaps. Their E_{opt} can be accurately determined by the intersection between the normalized absorption (EQE_{PV}) and emission (Electroluminescence, EL) spectra of the blend film (device),[30,31] or the mean peak energy from the derivatives of the EQE_{PV} curve.[32] A simple and rather close approximation for E_{opt} is the energy in the tail, corresponding to the half-maximum of the EQE_{PV}.[9] The thermodynamic PCE limit for single-junction solar cells calculated via Shockley–Queisser (S–Q) theory is also shown (dashed line). b) Plot of open-circuit voltage (V_{OC}) as a function of E_{opt}. Solid and dashed gray lines present E_{opt}/q and $E_{opt}/q-0.55$ V, respectively. The blue dashed line presents the radiative V_{OC} limit calculated via S–Q theory.

optical gap of the absorber (E_{opt}) and the experimentally measured open circuit voltage (V_{oc}) under 1-sun condition, that is, $E_{opt}/q- V_{oc}$, with q being the elementary charge. As shown in Figure 1b, the photo-voltages of GaAs and GaInP solar cells almost reach their radiative V_{OC} limit,[28] as predicted by Shockley and Queisser,[29] resulting in voltages losses close to 0.3 V, while much larger losses of ≈0.55 V are found for current OSCs. As compared to the best photovoltaic technologies, the current class of OSC materials loses approximately an additional 0.2–0.25 V of open-circuit voltage.

In the currently highest efficiency NFA-based OSCs, the voltage losses related to the photo-induced charge transfer process, converting singlet excitons to CT states are negligible, that is, $\Delta E_{S1,CT} \approx 0$. The total voltage losses are instead due to free carrier recombination, which has a radiative and non-radiative contribution. Radiative recombination via an electronic excited state which coupled to the ground-state, such as a singlet state or CT state is unavoidable and thus sets the thermodynamic upper limit to the open-circuit voltage, $V_{oc,\,rad}$. Additional non-radiative recombination lowers the measured open-circuit voltage, $V_{oc,\,exp}$ as compared to $V_{oc,\,rad}$, with a loss $\Delta V_{oc,\,nr}$, defined as

$$\Delta V_{oc,nr} = V_{oc,\,rad} - V_{oc,\,exp.} \quad (1)$$

In the case that all non-radiative channels are fully suppressed, $\Delta V_{oc,nr}$ will be zero and the device's open-circuit voltage equals $V_{oc,rad}$: The photovoltaic device will also be a good light-emitting diode with a theoretical electroluminescence external quantum efficiency (EQE_{EL}) of 100%. In general, the non-radiative voltage losses are quantified by the equation below,[39,40]

$$\Delta V_{oc,nr} \approx -\frac{k_B T}{q} \ln(EQE_{EL}) \quad (2)$$

where k_B is Boltzmann constant, and T is the temperature of the device.

Table 1 shows a comparison of the EQE_{EL} values for various photovoltaic technologies. The best NFA OSC has a $\Delta V_{oc,nr}$ of 240 mV, equivalent to an EQE_{EL} of ≈0.01% which is 2–3 orders of magnitude lower than that of the state-of-the-art inorganic devices. The low non-radiative voltage losses in the latter have been achieved by reducing trap-induced and surface recombination at the contact/active layer interface.[41,42] For OSCs, however, the radiationless decay pathways are less well understood. Non-radiative decay in optimized OSCs has been attributed to mechanisms intrinsic to organic semiconductors, rather than to extrinsic impurities or surface recombination at contacts. Intrinsic mechanisms are non-radiative decay via triplet states on donor and/or acceptor[43] and via internal

Table 1. Comparison of the photovoltaic parameters, voltage loss, $\Delta V_{oc,nr}$, and EQE_{EL} of selected record solar cells (see Ref. [33] for more details).

Material	E_{opt} [eV]	V_{OC} [V]	J_{SC} [mA cm^{-2}]	*FF* [%]	*PCE* [%]	$E_{opt}/q- V_{oc}$ [V]	$\Delta V_{oc,\,nr}$ [V]	EQE_{EL} [%]	Reference
c-Si	1.10	0.74	42.6	84.9	26.7	0.36	0.107	1.6	[34]
GaAs	1.43	1.12	29.8	86.7	29.1	0.31	0.027	35.7	[35]
CIGS	1.09	0.73	39.4	80.4	23.4	0.35	0.096	2.4	[36]
GaInP	1.85	1.49	16.3	87.7	21.4	0.35	0.053	13.0	[37]
Perovskite	1.53	1.19	26.4	81.7	25.6	0.34	0.059	10.1	[38]
Organic	1.45	0.89	26.7	80.8	19.2	0.56	0.24	0.01	[19]

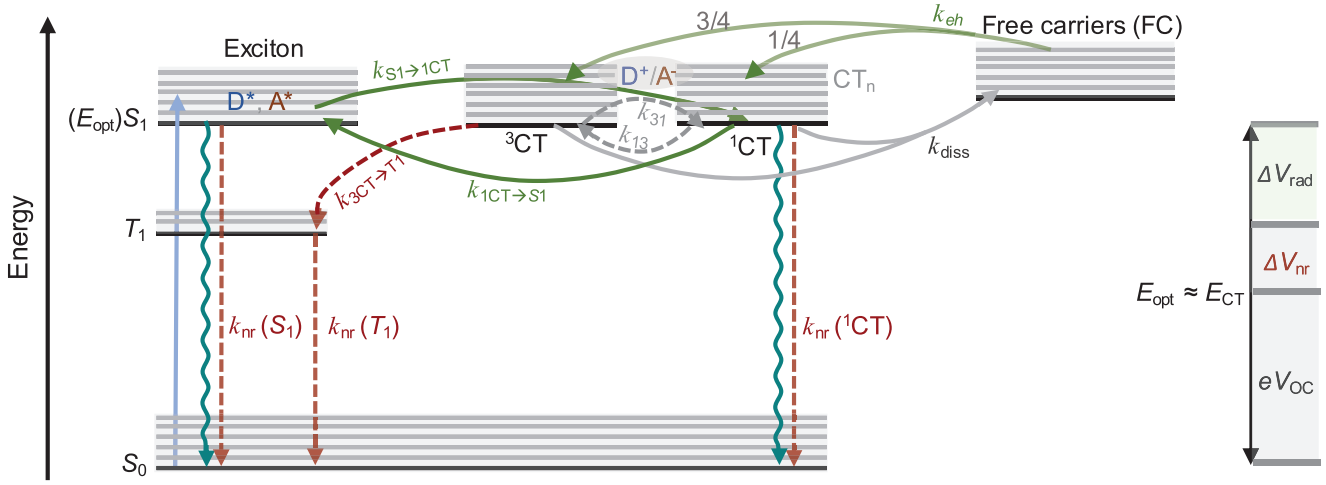

Figure 2. Jablonski diagram showing the possible radiative and non-radiative transitions at the donor–acceptor interface. In current non-fullerene OSCs, E_{CT} is almost equal to the optical gap (E_{opt}) or the energy of the lowest singlet (S_1) state of the lower gap component in the blend. Pathways for charge-carrier generation and recombination are indicated with arrows. Blue and red arrows present radiative and non-radiative recombination channels of the excited state species, respectively. On the right panel of the figure, the eenergy loss for NFA solar cells is indicated, mainly resulting from both radiative and non-radiative CT and S_1 state decay during charge recombination.

conversion of CT states to the ground-state governed by the "energy gap law".[44–47] Also the $\Delta E_{S1,CT}$ offset has been shown to play a role in determining $\Delta V_{oc,nr}$,[48–51] as well as the donor–acceptor blend morphology,[12,52–54] interfacial molecular orientation/packing,[55–57] energetic disorder,[58–61] and electroluminescence linewidth.[62]

In this review, we aim to give an overview of current understanding of the origin of non-radiative recombination in OSCs. We compare several characterization techniques for quantifying the related voltage losses and then highlight successful pioneering approaches to reduce non-radiative recombination losses in non-fullerene OSCs, including but not limited to new material design and morphological control. Finally, based on the current understanding, we provide an outlook on the design rules that should be taken into account to minimize non-radiative recombination losses while keeping an efficient photo-induced charge separation.

2. Charge Generation and Recombination Pathways in Non-Fullerene OSCs

2.1. Electronic State Diagram

Upon optical excitation of either the electron donating (D) or accepting (A) materials in the active layer of an OSC, the photogenerated exciton will diffuse to the D/A interface and create a CT state where the electron almost fully resides on A and the hole on D. Nowadays, most efficient polymer, NFA blends, the S_1 state of the NFA is the lowest energy local excitonic (LE) state. The donor is chosen such that the interfacial CT state is close in energy with the LE state, resulting in the formation of LE-CT hybrid state at the D/A interface, which subsequently dissociates efficiently into free carriers without hereby losing energy during the electron-transfer process.[63]

Depending on the excitation wavelength above the optical gap E_{opt} (the difference between S_0 and S_1 of the NFA), high energy singlet states in donor or acceptor are created. In their conversion process to free carriers, they will lose their excess energy, as shown in the Jablonski diagram of **Figure 2**. This can in principle occur via formation of higher energy CT states (CT_n) which then dissociate, giving the free carriers with some excess energy. Alternatively, relaxation from CT_n to the lowest energy CT state (CT_1) occurs via internal conversion, subsequently producing free carriers (FC) at high efficiency.[64] Under the built-in potential of a full device, these free carriers move toward the respective electrodes through the bi-continuous networks. This results in a photocurrent, which, depending on the applied voltage, results in a net flow of electrons out of the photovoltaic device. At open-circuit, no charge flows out of the devices and all photo-generated free carriers recombine. The balance between the photocurrent generation and free carrier recombination processes therefore determines the density of charge carriers, and thus their chemical potential at open-circuit, that is, the open-circuit voltage. In order to achieve the highest V_{OC}, the overall free carrier density at open circuit needs to be maximized, and thus the recombination rate minimized. The absolute lowest recombination rate is achieved when only radiative recombination is present.

In the following text, we focus on discussing the intrinsic non-radiative pathways, affecting the carrier density in the active layer at open-circuit. Trap-assisted recombination at extrinsic defects or interface recombination at the electrical contact layers with the active layer have been shown to affect OSC performance,[65,66,52] but are considered to form minor contributors to non-radiative recombination pathways in the highest performance OSCs. They are therefore not discussed in detail.

Figure 2 illustrates the main recombination processes for a low energy offset D/A bulk-heterojunction blend where the

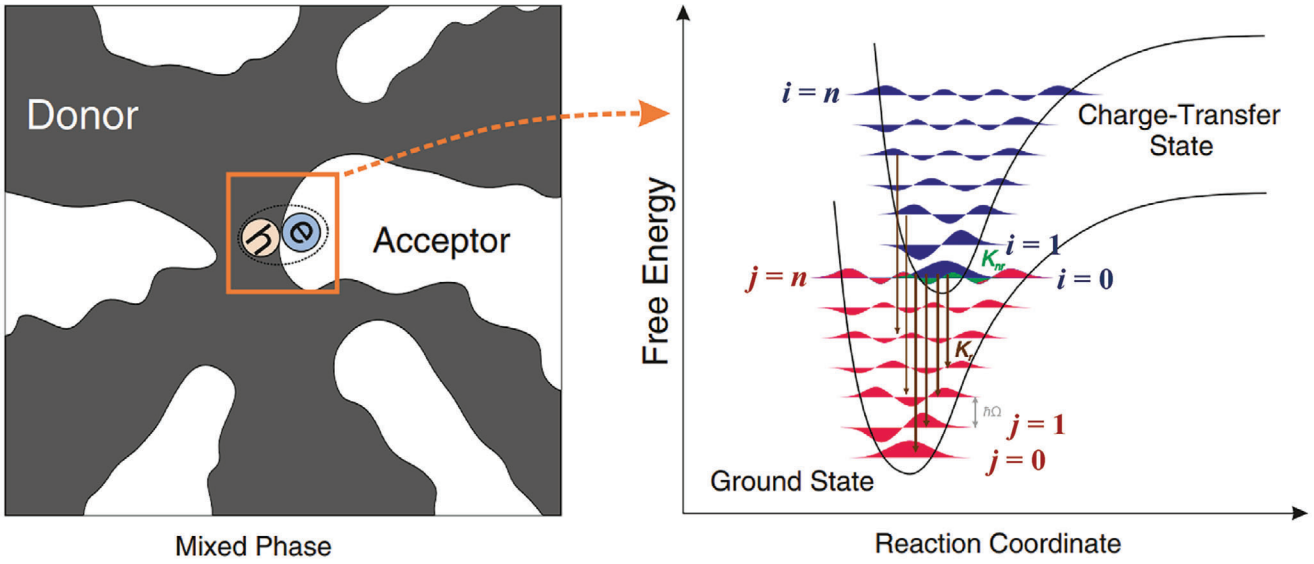

Figure 3. Non-radiative recombination mechanism in an OSC device. On the left panel: Schematic illustrating an interfacial CT state in a bulk-heterojunction system. On the right panel: Potential energies of the ground state and the CT state at the D/A interface as a function of the reaction coordinate. The quantized vibrational modes of the electronic ground state and CT state are shown as the red and blue colored waves, respectively. The green overlap between the lowest vibrational CT state ($i = 0$) and a vibrationally excited ground state ($j = n$) indicates the non-radiative recombination pathway. The transition probability is sketched by the green area being the wavefunction overlap of both states. The red arrows depict possible radiative decay pathways, the electron directly being transferred to the relaxed ground state or a low vibrational mode of the ground state. Reproduced with permission.[71] Copyright 2018, American Physical Society.

energy of the lowest singlet S_1 is close to CT_1 state energy. Free charge carrier recombination is a complex process, involving several electronic states, with dominant pathways currently debated. Based on current literature, the following picture emerges: Upon encounter of a free hole and electron at the donor–acceptor interface, CT states are formed. The singlet CT state (^{1}CT) is coupled to the ground-state and can decay radiative or radiationless (blue and red arrows, respectively). With the S_1 state almost iso-energetic with the ^{1}CT state, these states are expected to rapidly convert into each other, as is the case for a hybrid LE-CT state. There is, however, also a significant chance ^{1}CT re-dissociates into free carriers. Spin statistics dictate that the probability for ^{1}CT formation upon electron-hole encounter is 1/4, while the chance for formation of a triplet ^{3}CT state is 3/4. Triplet CT states are in principle not coupled to the ground state, but can convert to local triplet states T_1, on donor or acceptor, which then decay non-radiatively. Singlet and triplet CT states are expected to be nearly iso-energetic[67,68] and spin-flips occur via (reverse) intersystem crossing.

The overall recombination rate for free carriers thus depends not only on the electron-hole encounter rate ($k_{eh} = k_{eh\rightarrow 1CT} + k_{eh\rightarrow 3CT}$), but in a complex manner on the (re-)dissociation rate (k_{diss}), (reverse) intersystem crossing rates (k_{13}, k_{31}), ^{1}CT to S_1 interconversion rates ($k_{1CT\rightarrow S1}$ and $k_{S1\rightarrow CT}$), ^{3}CT to T_1 conversion rate ($k_{3CT\rightarrow T1}$) and decay rates of the CT state and S_1 state. The exact values of each of the rate constants indicated in Figure 2, are currently not known and likely depend on material system. There are indications that several of the excited states (free carriers, CT states, and singlet states) are in equilibrium with each other,[69] which means that conversion of (some) the excited states and free carriers into each other is much faster than the decay to the ground-state of CT and S1 states ($k_{13\rightarrow 31} >> k_{1CT}$ and k_{S1}). It has, for example, been observed that the overall free carrier recombination rate is strongly reduced in comparison with the free carrier encounter rate (so-called Langevin rate), which can be explained by CT states dissociating multiple times into free carriers, bringing CT states and free carriers in equilibrium with each other, before decaying.[70] The already complex picture shown in Figure 2 does not take into account disorder and due to the multiple excited states involved, conversion rates are difficult to determine and a topic of debate.

2.2. Molecular Parameters Determining Radiative and Non-Radiative Decay Rates

The overall free carrier density and thus V_{OC} depend in a complex way on the decay rates of the singlet and CT states (k_{1CT} and k_{S1}), as well as the interconversion rates between excited states (CT, singlet and triplet) and free carriers. In what follows, we consider CT state to ground-state internal conversion as dominating the total recombination and summarize briefly which molecular factors affect k_{1CT}. **Figure 3** depicts the potential energy parabola of the ground state and the CT state. The vibrationally relaxed CT state has a different conformation than the vibrationally relaxed ground state. Higher energy vibrational levels and their wave-functions in the harmonic approximation are depicted. In the Franck–Condon approximation is the radiative decay of the CT state proportional to the wave-function overlap between the lowest energy excited state ($i = 0$) and all vibrational modes ($j = 1,2,3, ...$) of the ground state, indicated by the red arrows in Figure 3. The non-radiative decay rate is on the other hand

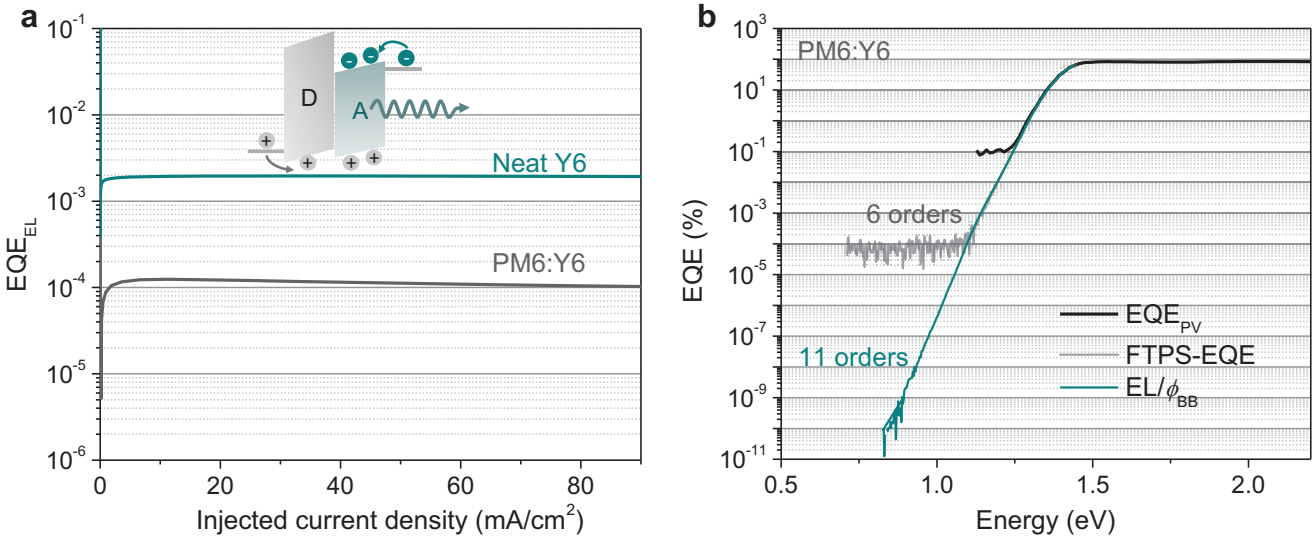

Figure 4. Accurate determination of non-radiative recombination voltage loss for OSC devices. a) $\Delta V_{oc,nr}$ derived from electroluminescent quantum yield (EQE_{EL}) measurement. The injected current density dependent EQE_{EL} curves of PM6:Y6 and neat Y6 devices are shown. Here, note that the EQE_{EL} value for calculating $\Delta V_{oc,nr}$ should be recorded at an injected current density equivalent to J_{SC} measured under AM1.5G illumination. b) $\Delta V_{oc,nr}$ derived from sensitive-EQE_{PV} measurement. Typical EQE_{PV} curves of the PM6:Y6 device are shown: Normal EQE_{PV} (black), FTPS-EQE (gray), and constructed EQE_{PV} (cyan) calculated using optoelectronic reciprocity.

proportional to the wave-function overlap between the lowest energy excited state ($i = 0$) and the iso-energetic vibrational mode of the ground state ($j = n$), indicated by the green coloured area in Figure 3.[45,71]

The wave-function overlap between the i and j vibrational states is given by the Franck–Condon factor weighted density of states FCWD(E), which accounts for transitions between all vibrational modes of the initial and the final state with the vibrational states differing in energy by E (see Ref. [71]),

$$\mathrm{FCWD}\,(E) = \frac{1}{\sqrt{4\pi\lambda_L k_B T}} \times \sum_{j=0}^{\infty}\sum_{i=0}^{\infty} \frac{e^{-S} S^{j-i} i!}{j!} \left[L_i^{j-i}(S)\right]^2 e^{\left(-\frac{(E-E_{CT}+\lambda_L+(j-i)*\hbar\Omega)^2}{4\lambda_L k_B T}\right)} e^{-i\hbar\Omega/k_B T} \quad (3)$$

with $\hbar$ the reduced Planck constant, λ_L the low frequency re-organisation energy, S is the Huang Rhys factor, being $\lambda_H/\hbar\Omega$, where $\hbar\Omega$ and λ_H are the vibronic spacing and re-organization energy of the high frequency modes, respectively. Both values of λ_L and λ_H are strongly dependent on the chemical structure of the materials. For organic semiconductors that contain many C-C bones, $\hbar\Omega$ has a typical value of 0.15 eV. $L_i^{j-i}(S)$is the generalized Laguerre polynomial of degree i. Using the electron transfer-rate constant expression, with Fermi's golden rule and the Born–Oppenheimer approximation, the non-radiative decay rate (k_{nr}) can be described below by a product of the electronic coupling V between the CT state and ground state and FCWD (0),[71]

$$k_{nr} = \frac{2\pi}{\hbar} V^2 \mathrm{FCWD}\,(0) \quad (4)$$

For E_{CT} sufficiently high, Equation (4) can be roughly approximated by:

$$k_{nr} \propto \exp\left[-\frac{E_{CT}-\lambda_L}{\hbar\Omega}\left\{ln\left(\frac{E_{CT}-\lambda_L}{\lambda_H}\right)-1\right\}-\frac{\lambda_H}{\hbar\Omega}\right] \quad (5)$$

This equation is known as the energy gap law: an exponential dependence of k_{nr} on the excited state energy, which in this case is E_{CT}. Since $\Delta V_{oc,nr}$ depends on EQE_{EL} (Equation 2), which is inversely proportional to k_{nr}, this law predicts that an organic photovoltaic device with higher E_{CT} should have reduced non-radiative voltage losses. This is indeed observed for fullerene-based devices.[46] When LE-CT hybridization is taken into account the dependence on E_{CT} becomes more complex (see Ref. [47]). Nevertheless, at very high E_{CT}, in the visible region ≈2.4 eV, it has been shown that EQE_{EL} can be above 1%, which is 100–1000 times higher than typical EQE_{EL} values of NFA cells with optical gaps in the near-infrared, ≈1.4 eV. This results in $\Delta V_{oc,nr}$ of 90–130 meV and a V_{oc} approaching S-Q limit for visible light emitting organic photovoltaic devices.[72] However, for efficient light harvesting, the energy gap should be in the 1.1–1.5 eV range. In order to reduce k_{nr}, increase EQE_{EL} and reduce $\Delta V_{oc,nr}$, the other parameters of Equations (3)–(5) need to be tuned, being λ_L, λ_H, the dominant vibrational mode $\hbar\Omega$ and electronic coupling from CT state to ground state. These parameters are affected by the molecular structures of donor and acceptor, film morphology, molecular orientation, packing, etc. Promising strategies leading to experimentally verified reductions in $\Delta V_{oc,nr}$ will be further discussed in Section 4.2. But first, we summarize how to accurately and correctly determine $\Delta V_{oc,nr}$ using experimental data.

3. Accurate Determination of Non-Radiative Voltage Losses

Having discussed recombination pathways in state-of-the-art NFA solar cells, we now turn to provide an accurate way to experimentally quantify the non-radiative voltage loss, $\Delta V_{oc,\,nr}$. In this section, we show two well-established approaches to characterize such loss, as seen in **Figure 4**, and discuss the limitation of each method.

As $\Delta V_{oc,nr}$ can be quantified using Equation (2), experimentally measuring the EQE_{EL} of a complete OSC is becoming a popular and rather easy way to characterize voltage losses. Generally, EQE_{EL} depends on the charge carrier density. Therefore, to ensure that the obtained $\Delta V_{oc,nr}$ is relevant and correct, the EQE_{EL} value should be recorded at a charge density in the device, comparable to 1 sun, open-circuit conditions. This means that the injected current density during the EQE_{EL} measurement should be comparable to J_{SC} measured under AM1.5G illumination or that the applied voltage during the measurement does not substantially exceed typical V_{OC} values. Note that when a too large bias (or current density) is applied, a large deviation of the charge carrier density from quasi-equilibrium conditions may result in a higher determined radiative efficiency, and thus an overestimated EQE_{EL} value.[73,74] From the Equation (2), one can estimate that the $\Delta V_{oc,nr}$ decreases by ≈60 mV each time when the EQE_{EL} is enhanced by one order of magnitude. As seen in Figure 4a, bringing the EQE_{EL} value of 10^{-4} of the current workhorse donor–acceptor blend, PM6:Y6, close to that of neat Y6 film (EQE_{EL}≈10^{-3}), an ≈60 mV gain in V_{oc} would be expected. In our previous work, indeed, this occurred when low-molecular-weight fractions of the polymer PM6 was used, improving the V_{OC} of PM6:Y6 devices from the typical values of 0.84 V to above 0.9 V.[62]

While various other research groups have validated Equation (2),[49,75] some caution when measuring EQE_{EL} for voltage loss determinations is required: If the applied forward voltage over the device during measurement is too high, charge injection more easily excites the pure domains of donor or acceptor in the blend, especially when the CT energy is very close to the S_1 states. As a consequence, the measured EQE_{EL} overestimates the value relevant in Equation (2). The D18:PMI-FF-PMI (E_{opt} = 2.02 eV) system, reported by Hofinger et al.,[76] is a good example here. The experimentally measured EQE_{EL} of the OSC device is as high as 0.1%, while the calculated EQE_{EL} value derived from the non-radiative voltage loss analysis discussed below, is only 0.006%, yielding an ≈70 mV underestimation of the $\Delta V_{oc,nr}$ value. A similar underestimation of $\Delta V_{oc,nr}$ values within a range of 30–80 mV from EQE_{EL} measurements has been observed for several wide-gap (>1.8 eV) NFA-based OSCs.[77–80]

The EQE_{EL} value is strongly affected by the applied bias and charge injection balance, occasionally leading to the unreliable determination of $\Delta V_{oc,nr}$ if the injected charge densities and distribution differ substantially from the conditions at V_{oc} under 1-sun. We therefore recommend performing these measurements at rather low injections currents, as they mimic V_{oc} conditions the best.

A more reliable $\Delta V_{oc,nr}$ value is obtained using an analysis based on a detailed balance approach: The radiative limit, $V_{oc,\,rad}$ can be calculated using the following equation,[81]

$$V_{oc,rad} = \frac{k_B T}{q} In\left(\frac{\int EQE_{PV}(E)\times\phi_{AM1.5}(E)\,dE}{\int EQE_{PV}(E)\times\phi_{BB}(E)\,dE}+1\right) \quad (6)$$

where $\phi_{AM1.5}(E)$ and $\phi_{BB}(E)$ are the AM 1.5G solar irradiation and Plank's black-body radiation spectrum at the device's temperature T, respectively. For the latter, $\phi_{BB}(E)$ is given by

$$\phi_{BB}(E) = \frac{2\pi E^2}{h^3c^2}\frac{1}{\left(exp\left(E/k_B T-1\right)\right)} \quad (7)$$

where h is Planck's constant, and c is speed of light in vacuum. The product $EQE_{PV}(E)\times\phi_{BB}(E)$ depends strongly on the low energy part of the EQE_{PV} spectrum. Therefore, in order to evaluate $V_{oc,rad}$ using Equation (6), a sensitive measurement of the EQE_{PV}(E) spectrum in the low energy tail and sub-gap region is required. Such measurements can be obtained using a lock-in technique or via Fourier transform photocurrent spectroscopy (FTPS) measurements.[82,83] As shown in Figure 4b, the FTPS technique allows for measurement in the sub-gap regime as low as EQE_{PV} ≈10^{-6} for PM6:Y6 cells.

The $EQE_{PV}(E)$ tail and the electroluminescence (EL) spectrum of the device at low injection voltages are related by a reciprocity relation: $EQE_{PV}(E) \approx EL(E)/\phi_{BB}(E)$.[39,84] Figure 4b shows the validity of this relation for PM6:Y6: The $EL(E)/\phi_{BB}(E)$ overlaps with the measured $EQE_{PV}(E)$ spectrum and extends it further into the sub-gap region by more than 5 orders of magnitude[75] This reconstructed $EQE_{PV}(E)$ spectrum is used to accurately evaluate the integral in the denominator of Equation (6). With knowledge of $V_{oc,rad}$, the non-radiative voltage losses can be calculated using Equation (1): $\Delta V_{oc,nr} = V_{oc,\,rad} - V_{oc,\,exp.}$. Note that the $\Delta V_{oc,nr}$ derived from both EQE_{EL} and FTPS-EQE techniques coincide if EQE_{EL} is measured under the correct injection conditions, mimicking charge densities close to V_{oc} conditions.

4. Approaches to Suppress Non-Radiative Recombination Losses in OSCs

4.1. The Need for NFAs with a High Photoluminescence Quantum Efficiency

The currently best non-fullerene OSCs have an EQE_{PV} ≈85% and a FF >80%. Reduction of $\Delta V_{oc,nr}$ (or increase in EQE_{EL}) would boost the efficiency above 20%. In this section, we will discuss the recent advances in reducing the non-radiative recombination loss and relevant strategies are summarized below.

The EQE_{EL} of the device is limited by the photoluminescence quantum yield (PLQY) of donor: NFA blend films, which can reach a few percent.[49,62,85] In the typical case that the NFA is the low gap component of the blend, its PLQY limits in turn the blends' PLQY. Thus, to further improve the PLQY values of blend films, NFAs with high PLQYs should be selected and their emissive properties should be enhanced. As efficient organic solar

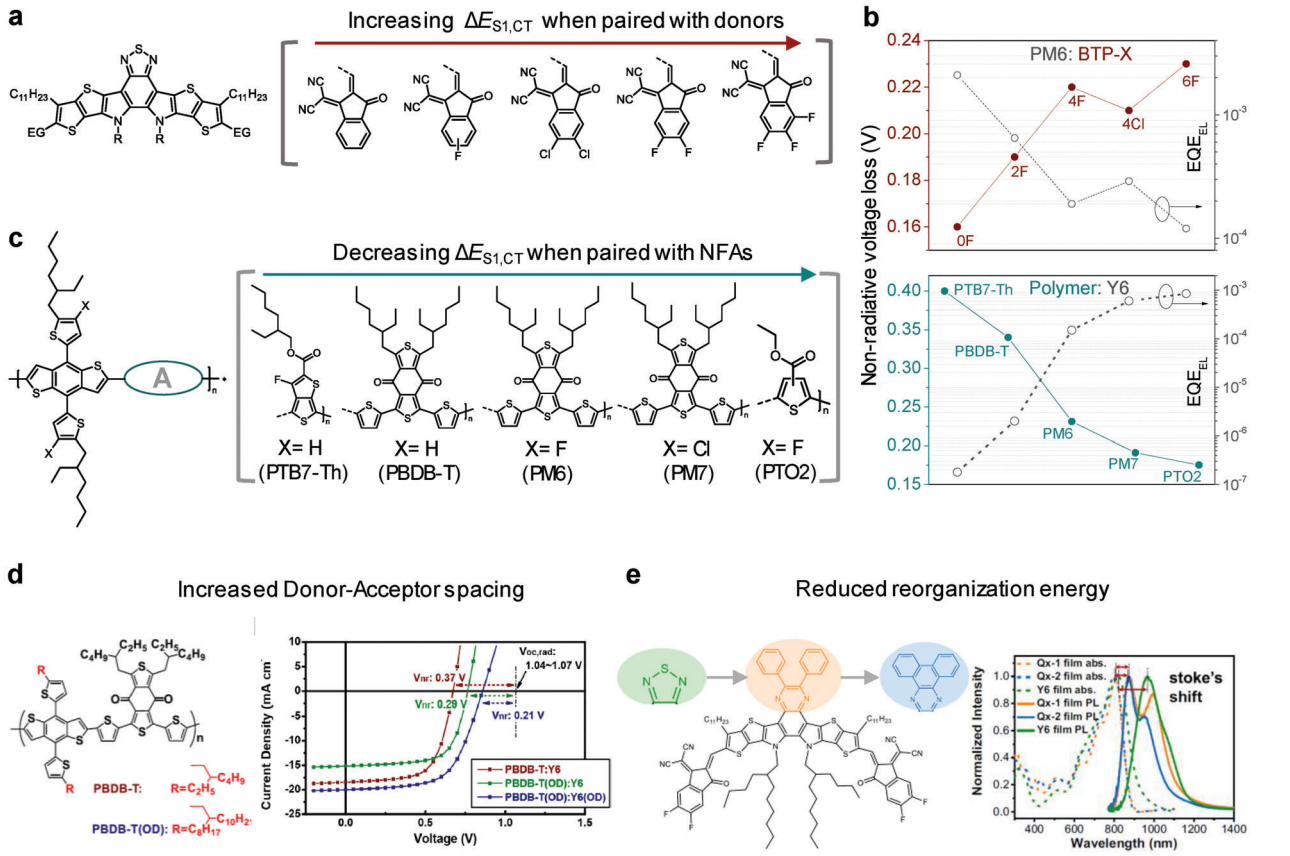

Figure 5. Reducing non-radiative losses by material design. a) Molecular structures of NFAs with a BTP core and different symmetrical end-groups, featuring a gradually increasing $\Delta E_{S1,CT}$ when paired with the PM6 polymer donor. b) Non-radiative recombination losses (solid) and EQE$_{EL}$ (dotted) for various PM6: NFA with increasing $\Delta E_{S1,CT}$ (top panel) and various polymer:Y6 blends with decreasing $\Delta E_{S1,CT}$ (bottom panel). c) Molecular structures of polymer donor materials containing a fluorinated-thienyl benzodithiophene (BDT-2F) unit and different electron-accepting units, featuring gradually reduced $\Delta E_{S1,CT}$ when paired with the Y6 NFA. d) polymers based on the PBDB-T chemical structure, aiming to increase their spacing with Y6 derivatives. The current density–voltage curves of their corresponding devices are shown on the right side. Reproduced with permission.[98] Copyright 2021, Springer Nature. e) Newly designed Y6 derivatives with reduced re-organization energy. Left: chemical structures of NFA molecules. Right: absorption and photoluminescence spectra of the studied NFA thin-films, indicating a smaller Stokes shift compared to standard Y6. Reproduced with permission.[99] Copyright 2022, Springer Nature.

cells require an optical gaps in the near infrared (NIR), it is therefore useful to take a closer look at PLQY and EQE$_{EL}$ data reported for recent near-infrared light-emitting diodes (NIR-OLED).[86,87] The EQE$_{EL}$ values (0.2–0.5%) of pure NFA neat film-based devices have already approached the best solution-processed fluorescent organic emitters with an emission peak around 900 nm. Therefore, the design criteria or strategy for developing more efficient emitters used for NIR-OLEDs in the future, might also have potential for low voltage loss OSCs.

In fluorescent OLEDs, non-emissive triplet states are a main cause for a reduced EQE$_{EL}$. Also in OSCs, triplets are therefore expected to play a role in the recombination mechanism.[43,68] Gillett et al. demonstrated that in the PM6:Y6 system ≈90% of free charge recombination proceeds via the T_1 state of Y6.[43] Avoidance of that non-radiative loss channel would enhance the EQE$_{EL}$ by a factor of 10, and thus reduce $\Delta V_{oc,nr}$ by 60 mV. To practically realize this, the formation of triplet CT states (k_{13}, in Figure 2) or the back electron transfer $k_{3CT\rightarrow T1}$ should be suppressed. A reduced formation of triplets can be achieved by bringing the CT and local exciton states close in energy and by increasing the electronic coupling between them. This can result in a destabilized triplet CT state of which the energy is higher than that of the singlet CT state. In this case, population of triplet CT states and conversion to local triplet states is less favorable and thus recombination via T1 of the NFA phase can be suppressed.[88,89]

4.2. Material Design Guidelines for Reducing Non-Radiative Recombination Losses

An approach followed by several groups is to narrow the energy offset $\Delta E_{S1,CT}$ for a given D/A blend in which the highest occupied molecular orbital (HOMO) energy levels are sufficiently close to result in a strong electronic coupling between the CT state and the lowest S_1 excited singlet state (see Refs. [48,90,91]). This is achieved by tuning the frontier energy levels of D and A materials via the modification of their molecular skeletons, that is, introduction of Fluorine (F) or Chloride (Cl) electron-withdrawing elements. As shown in **Figure 5**a,

an increase in the number of F atoms on the end groups of BTP core-based non-fullerene acceptors leads to gradual downshift of their HOMO level. Using Cl slightly lowers the HOMO level even further as compared to the F-counterparts due to its higher electron-withdrawing nature. Pairing the series of NFAs shown in Figure 5a with the PM6 polymer donor decreases $\Delta E_{S1,CT,}$ which results in a decrease (increase) in $\Delta V_{oc,nr}$ (EQE_{EL}) (Figure 5b, upper panel). When $\Delta E_{S1,CT}$ is manipulated via tuning of the polymer HOMO level, a similar observation can be made: Figure 5c shows a series of donor polymers containing a BDT-2F unit combined with various acceptor units. When blending these polymers with Y6, the corresponding non-radiative losses correlate with $\Delta E_{S1,CT}$ (see Figure 5b, bottom panel). In general, lowering $\Delta E_{S1,CT}$ via backbone modification, side chain engineering,[92,93] or ternary polymerization,[94–97] lowers the voltage losses related to the conversion of singlet excitons to CT states. Once these losses are close to zero ($E_{CT} \approx E_{opt}$), a further tuning of frontier energy levels, bringing the HOMO of the donor and NFA close to each other, results in an increased EQE_{EL} and lower non-radiative voltage losses.

Recently, two voltage loss reduction strategies beyond the tuning of frontier energy levels have been experimentally demonstrated. The first one involves the design of a blend with an increased spacing between the donor polymer and NFA acceptor.[98] A careful manipulation of the D-A spacing using longer side chain on the PM6 polymer was shown to improve V_{oc} by a reduction of the non-radiative losses, without hereby significantly adjusting the frontier energy levels of the used materials (Figure 5d).

A second strategy is to reduce the re-organization energies (λ_L and λ_H) of the used materials, which reduces the Stokes shift between absorption and emission peaks, as well as the absorption tail steepness and, according to Equation (3), the non-radiative decay rate: Wei et al.[99] reported fused hetero-aromatic Qx derivatives based on the Y6 molecular backbone, with a reduced Stokes shift (Figure 5e) as compared to that of Y6 molecule, suggesting a reduced molecular re-organization energy. This enabled a device efficiency over 18% with a $\Delta V_{oc,nr}$ of less than 0.2 V.

4.3. Morphology Control for Reducing Non-Radiative Recombination Losses

In addition to the approaches relying on newly synthesized materials, morphology control of a given blend and its effect on non-radiative voltage losses has been explored. The heterogeneity of local morphologies in bulk-heterojunctions in terms of D-A blend ratio, different molecular weight polymers, additives, growth, and annealing conditions strongly influences the energy levels and dynamics of interfacial CT states,[54,100] and thus voltage losses in general. An often observed trend is that a more aggregated morphology leads to relatively larger non-radiative losses,[9,24,101,102] which could be ascribed to reduced fluorescence emission efficiency[103] and/or increased the local D-A HOMO offset in the aggregated solid state.[104] Preventing aggregation of NFAs by dispersing them into a polymer: fullerene matrix has been shown to reduce $\Delta V_{oc,nr}$.[105,106] As shown in **Figure 6**c, when a large weight loading of $PC_{61}BM$ fullerene material accounting for 90% of the total acceptor is mixed into the PM6:Y6 blend, indicating the Y6 aggregates are well diluted and dispersed, as a result, such ternary device has a reduced non-radiative energy losses compared to that of PM6:Y6.[105]

Alternatively aggregation can be tuned by using various-molecular-weight fractions of PM6 in blends with NFAs.[62] The low molecular weight fractions of PM6 result in a less aggregated PM6 and NFAs domains, and as a result, the device EQE_{EL} is enhanced and approaches that of a neat NFA device for several blend systems, hereby reducing the corresponding $\Delta V_{oc,nr}$. The latter correlates well with the EL emission linewidths (in *eV*s) for a large set of devices (Figure 6b). A narrower emission linewidth is an indication of a lower re-organization energy or reduced energetic disorder. Recently, several studies correlated Urbach energies (E_u) extracted by exponentially fitting the sensitively measured EQE tail with device voltage losses.[9,107–109] However, some care needs to be taken when determining E_u from these spectra: Optical interference effects can strongly affect the shape of the absorption tail,[110–112] which is further determined by exciton and CT state properties in a complex way. Not taking this into account would result in an unfair comparison between different systems. For current low HOMO-offset blends in which the CT state spectral feature is absent, it is further unclear how the energetic disorder of the exciton density of states determining the sharpness of the tail would affect $\Delta V_{oc,nr}$.[113] Nevertheless, the static disorder of CT states has recently been shown to have influence on both $V_{oc,rad}$ and $\Delta V_{oc,nr}$ by Nelson and coworkers.[114] Later, Rand et al. [60] also have shown a correlation between the CT-state disorder and non-radiative loss: In a study on serval planar and bulk heterojunction OSCs it was found that $\Delta V_{oc,nr}$ quadratically increases with an increasing CT-state energetic disorder parameter (Figure 6c). Nelson and co-workers design rules on how to reduce CT state disorder by morphology tuning are however not established yet.

Besides aggregation within the donor and acceptor phase, the relative orientation of the different phases at the donor/acceptor interfaces has been shown to influence $\Delta V_{oc,nr}$. As shown in Figure 6d, Nguyen et al.[115] reveal that the molecular orientation of p-SIDT$(FBTTh_2)_2$ in the neat film has a profound effect on the device V_{oc} (see the *J*–*V* curves). A much larger V_{oc} is observed for the device with p-SIDT$(FBTTh_2)_2$ face-on orientation, which results in a higher CT energy and less non-radiative recombination losses. A similar trend is observed in solution-processed all-small-molecule non-fullerene OSCs.[116] When the length of the alkyl side-chain on the DRTB-TX donor molecule increases, the molecular orientation relative to the substrate changes from mainly edge-on to face-on and the corresponding V_{oc} of devices based on DRTB-TX:IT-4F blends increases from 0.89 to 0.93 V. Also, for all-polymer OSCs, orientation affects the voltage losses. Ma et al. fabricated P3HT (D)/N2200 (A) bilayer devices with different molecular orientations that are controlled by employing various solvents and thermal annealing.[117] When P3HT has a face-on orientation, which has an ≈50 mV higher V_{oc} than of the edge-on case is obtained. In contrast, when N2200 is face-on orientated, an extra recombination loss appears, reducing V_{oc}. Hence, molecular orientation of both D and A phases manipulates recombination energy losses, and thus device performance. In the future, a deeper understanding of the relation between molecular orientation and device performance would be valuable,

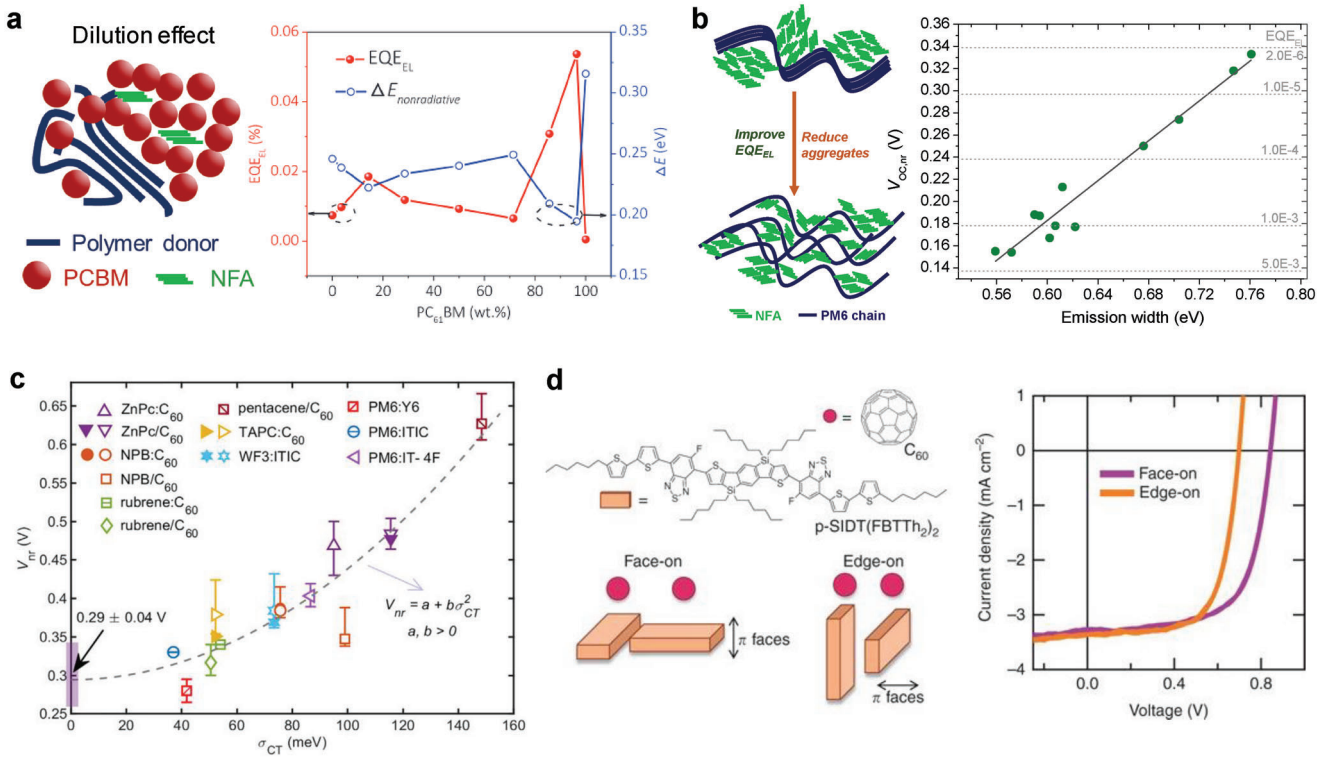

Figure 6. Morphology and energetic disorder control for reducing non-radiative recombination losses. a) Left: schematic drawing of the dilution effect. Right: Plot of $\Delta V_{oc,nr}$ and EQE_{EL} for PM6:Y6 ternary devices with different loadings of $PC_{61}BM$ at a fixed D:A weight ratio of 1:1.4. Reproduced with permission.[105] Copyright 2019, Wiley-VCH. b) Left: schematic drawing of a morphology with reduced aggregation. Right: correlation between the linewidth (in *e*V) of the emission spectrum and $\Delta V_{oc,nr}$ for PM6-based devices with different non-fullerene acceptors. Reproduced with permission.[62] Copyright 2021, Elsevier. c) Correlation between $\Delta V_{oc,nr}$ with CT-state disorder (σ_{CT}) at room temperature. Reproduced with permission.[60] Copyright 2022, Elsevier. d) Molecular orientation of p-SIDT$(FBTTh_2)_2$ and C_{60} in the face-on and edge-on bilayer samples, and the resulting photovoltaic performance. As shown in the *J*–*V* curves, the face-on orientation of the donor molecule has a larger V_{oc}, resulting in a reduced non-radiative loss. Reproduced with permission.[115] Copyright 2017, Springer Nature.

as well as strategies for precisely controlling the orientation in each phase.[118]

5. Trade-Off between EQE_{PV} and $\Delta V_{oc,nr}$ in Low Energetic-Offset Systems

Strategies described in the literature that successfully reduce $\Delta V_{oc,nr}$ unfortunately often have a negative impact on the EQE_{PV} and hereby the overall photovoltaic performance for both fullerene and NFA-based OSCs.[6,119] Reducing (non-radiative) voltage losses by reducing $\Delta E_{S1,CT}$ via frontier energy level tuning in fullerene OSCs often results in a reduced free charge carrier generation yield. Efficient free charge carrier generation was therefore believed to require a considerable amount of driving force. This was challenged when He et al.[120] reported the first example of an NFA-based system, demonstrating fast and efficient charge separation with a negligible $\Delta E_{S1,CT}$ and an internal quantum efficiency (IQE) of nearly 90%. Also, the current workhorse PM6:Y6 blend, which has an IQE of ≈95%, does not show a significant $\Delta E_{S1,CT}$. The energetic difference between the HOMO levels of PM6 and Y6 is almost zero according to the traditional cyclic voltammetry (CV) or ultraviolet photoelectron spectroscopy (UPS) measurements. It is hereby however important to note that using above techniques it is difficult to determine the energy levels of D and A directly at the interface in the bulk-heterojunction, leading to uncertainty in the exact value of the HOMO levels.[121]

Figure 7a, reproduced from Classen et al.,[122] plots the maximum EQE_{PV} value as well as $\Delta V_{oc,nr}$ as a function of the difference between the HOMO of the donor and the acceptor, $\Delta E_{HOMO,}$ for several donor: acceptor combinations. It reveals the trend of a strongly decreasing $\Delta V_{oc,nr}$ when ΔE_{HOMO} is tuned to small values, as seen in the intermediate regime in which the proposed Boltzmann stationary-state equilibrium between CT states and excitons (CT-LE equilibrium) manipulates the $\Delta V_{oc,nr}$. Especially when ΔE_{HOMO} is less than an empirical threshold value of ΔE_{HOMO} ≈0.2 eV, both $\Delta V_{oc,nr}$ and EQE_{PV} decrease steeply with Y6 as exception. A rather large number of studies observe a similar trend: Reducing ΔE_{HOMO} enables a smaller $\Delta V_{oc,nr}$, but comes at the expense of EQE_{PV}, FF, and overall efficiency of the device.[47,90,123,51,124] So far, the fundamental reason why the PM6:Y6 device can maintain such a high EQE_{PV} at such low ΔE_{HOMO} is not clear. An explanation given by Classen[122] is the significantly improved exciton lifetime in Y6 NFA as compared to PCBM-based systems, up to 1 ns, which gives more time for exciton dissociation, making it more efficient.

For the recently reported high efficiency OSCs using NFAs from the Y-series, EQE_{EL} values are approaching those of the

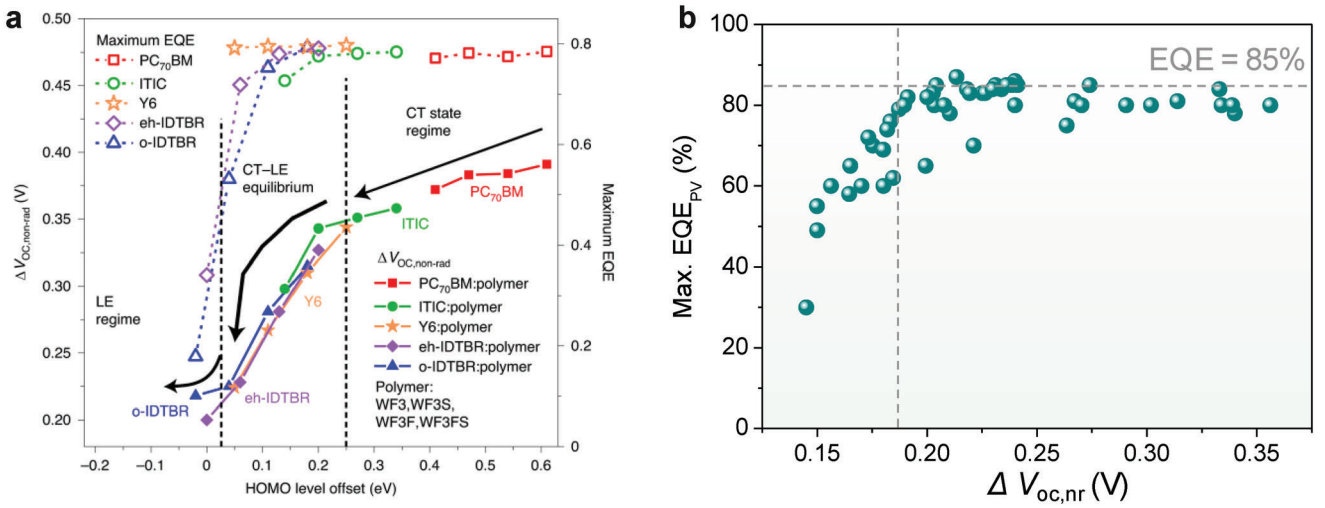

Figure 7. Correlation between non-radiative voltage loss and charge generation yield in low energetic offset systems. a) Analysis of $\Delta V_{oc,nr}$ and maximum EQE_{PV} of devices as a function of the HOMO level offset between D and A materials. Three perspectives in the left and right regimes $\Delta V_{oc,nr}$ are solely determined by the local exction (LE) and CT state properties, respectively. In the intermediate regime, the CT–LE equilibrium determines $\Delta V_{oc,nr}$. Reproduced with permission.[122] Copyright 2017, Springer Nature. b) Plot of maximum EQE_{PV} as a function of $\Delta V_{oc,nr}$ for over 50 NFA-based OSCs using Y-series acceptors.

neat NFA. However, a trade-off between $\Delta V_{oc,nr}$ (and thus EQE_{EL}) and maximum EQE_{PV} values remains, as shown in Figure 7b. For more than 50 recently published Y-series-based OSC devices, $\Delta V_{oc,nr}$ varies over 200 mV (from 0.15 to 0.35 V). Once $\Delta V_{oc,nr}$ is less than 0.18 V, corresponding to an EQE_{EL} of more than 0.1%, the peak EQE_{PV} drops rapidly below 80%. Hence, to further improve OSC efficiency, the physical origin of this trade-off needs to be urgently addressed and mitigated. That will require newly designed material systems with long-lived and disorder-free CT- and excitonic states with low reorganization energies.[125–127]

6. Conclusion and Future Perspective

We have summarized the recent efforts undertaken to understand the origin of non-radiative recombination losses in NFA-based OSCs and discussed some empirical strategies to reduce them. It is clear that the community is still at the early stages of understanding the fundamental factors controlling non-radiative recombination processes at D-A interfaces and $\Delta V_{oc,nr}$ has been eliminated only partially. No doubt, substantial efforts will be needed and future strategies developed for efficient NIR-OLEDs may be adapted for OSCs since they are sharing the same goal of improving EQE_{EL}. In contrast to NIR-OLEDs, however, efficient OSC additionally require a well-designed blend morphology with high and balanced electron and hole mobilities, strong light absorption, and an efficient CT state dissociation rate, resulting in high EQE_{PV}s, photocurrents, and FFs.

Once the above strategies are put into action, we are optimistic that non-fullerene OSCs can achieve PCEs close to the state-of-the-art inorganic or perovskite PVs. Indeed, a rather small $\Delta V_{oc,nr}$ value of ≈0.15 V (EQE_{EL} ≈ 0.3%) has been achieved when we used a NIR emitting NFA with a rather narrow electroluminescence linewidth (Ref. [62]). If this EQE_{EL} value could be achieved for the currently best OSC, an additional 90 mV enhancement in V_{oc} would result, giving over 21% efficiency. However, an important requirement is that the electronic states at the D-A interface do not only dissociate efficiently into free carriers, but also that the non-radiative paths for decay of these states are strongly supressed.

Acknowledgements

The authors acknowledge financial support from the European Research Council (ERC, grant agreement 864625) and the European Union's Horizon 2020 research and innovation program under the Marie-Curie grant agreement no. 882794.

Note: The second full affiliation for author Quan Liu was added; Figures 1–7 were reset; and Equation (3) was corrected, all on September 1, 2023, after initial publication online.

Conflict of Interest

The authors declare no conflict of interest.

Keywords

charge-transfer state, electroluminescence quantum efficiency, non-radiative recombination, open-circuit voltage loss, organic photovoltaic

Received: March 16, 2023
Revised: April 26, 2023
Published online: July 31, 2023

[1] M. C. Scharber, *Adv. Mater.* **2016**, *28*, 1994.
[2] J. Zhao, Y. Li, G. Yang, K. Jiang, H. Lin, H. Ade, W. Ma, H. Yan, *Nat. Energy* **2016**, *1*, 15027.
[3] D. C. Coffey, B. W. Larson, A. W. Hains, J. B. Whitaker, N. Kopidakis, O. V. Boltalina, S. H. Strauss, G. Rumbles, *J. Phys. Chem. C* **2012**, *116*, 8916.

[4] F. Gao, O. Inganäs, *Phys. Chem. Chem. Phys.* **2014**, *16*, 20291.
[5] A. J. Ward, A. Ruseckas, M. M. Kareem, B. Ebenhoch, L. A. Serrano, M. Al-Eid, B. Fitzpatrick, V. M. Rotello, G. Cooke, I. D. W. Samuel, *Adv. Mater.* **2015**, *27*, 2496.
[6] W. Li, K. H. Hendriks, A. Furlan, M. M. Wienk, R. A. J. Janssen, *J. Am. Chem. Soc.* **2015**, *137*, 2231.
[7] A. A. Bakulin, A. Rao, V. G. Pavelyev, P. H. M. van Loosdrecht, M. S. Pshenichnikov, D. Niedzialek, J. Cornil, D. Beljonne, R. H. Friend, *Science* **2012**, *335*, 1340.
[8] J. Yuan, Y. Zhang, L. Zhou, G. Zhang, H.-L. Yip, T.-K. Lau, X. Lu, C. Zhu, H. Peng, P. A. Johnson, M. Leclerc, Y. Cao, J. Ulanski, Y. Li, Y. Zou, *Joule* **2019**, *3*, 1140.
[9] S. Liu, J. Yuan, W. Deng, M. Luo, Y. Xie, Q. Liang, Y. Zou, Z. He, H. Wu, Y. Cao, *Nat. Photon.* **2020**, *14*, 300.
[10] J. Jin, Q. Wang, K. Ma, W. Shen, L. A. Belfiore, X. Bao, J. Tang, *Adv. Funct. Mater.* **2023**, *33*, 2213324.
[11] D. Luo, W. Jang, D. D. Babu, M. S. Kim, D. H. Wang, A. K. K. Kyaw, *J. Mater. Chem. A* **2022**, *10*, 3255.
[12] H. Hoppe, N. S. Sariciftci, *J. Mater. Res.* **2004**, *19*, 1924.
[13] H. Yu, Z. Qi, J. Zhang, R. Sun, Y. Chang, H. Sun, W. Zhou, J. Min, H. Ade, H. Yan, *J. Mater. Chem. A* **2020**, *8*, 23756.
[14] A. Armin, W. Li, O. J. Sandberg, Z. Xiao, L. Ding, J. Nelson, D. Neher, K. Vandewal, S. Shoaee, T. Wang, H. Ade, T. Heumüller, C. Brabec, P. Meredith, *Adv. Energy Mater.* **2021**, *11*, 2003570.
[15] J. Hou, O. Inganäs, R. H. Friend, F. Gao, *Nat. Mater.* **2018**, *17*, 119.
[16] C. Yan, S. Barlow, Z. Wang, H. Yan, A. K. Y. Jen, S. R. Marder, X. Zhan, *Nat. Rev. Mater.* **2018**, *3*, 18003.
[17] J. Wang, P. Xue, Y. Jiang, Y. Huo, X. Zhan, *Nat. Rev. Chem.* **2022**, *6*, 614.
[18] P. Murugan, T. Hu, X. Hu, Y. Chen, *J. Mater. Chem. A* **2022**, *10*, 17968.
[19] L. Zhu, M. Zhang, J. Xu, C. Li, J. Yan, G. Zhou, W. Zhong, T. Hao, J. Song, X. Xue, Z. Zhou, R. Zeng, H. Zhu, C. C. Chen, R. C. I. MacKenzie, Y. Zou, J. Nelson, Y. Zhang, Y. Sun, F. Liu, *Nat. Mater.* **2022**, *21*, 656.
[20] Y. Wei, Z. Chen, G. Lu, N. Yu, C. Li, J. Gao, X. Gu, X. Hao, G. Lu, Z. Tang, J. Zhang, Z. Wei, X. Zhang, H. Huang, *Adv. Mater.* **2022**, *34*, 2204718.
[21] P. Bi, S. Zhang, Z. Chen, Y. Xu, Y. Cui, T. Zhang, J. Ren, J. Qin, L. Hong, X. Hao, J. Hou, *Joule* **2021**, *5*, 2408.
[22] W. Gao, F. Qi, Z. Peng, F. R. Lin, K. Jiang, C. Zhong, W. Kaminsky, Z. Guan, C.-S. Lee, T. J. Marks, H. Ade, A. K.-Y. Jen, *Adv. Mater.* **2022**, *34*, 2202089.
[23] D. Li, N. Deng, Y. Fu, C. Guo, B. Zhou, L. Wang, J. Zhou, D. Liu, W. Li, K. Wang, Y. Sun, T. Wang, *Adv. Mater.* **2023**, *35*, 2208211.
[24] J. Fu, P. W. K. Fong, H. Liu, C.-S. Huang, X. Lu, S. Lu, M. Abdelsamie, T. Kodalle, C. M. Sutter-Fella, Y. Yang, G. Li, *Nat. Commun.* **2023**, *14*, 1760.
[25] C. He, Y. Pan, Y. Ouyang, Q. Shen, Y. Gao, K. Yan, J. Fang, Y. Chen, C.-Q. Ma, J. Min, C. Zhang, L. Zuo, H. Chen, *Energy Environ. Sci.* **2022**, *15*, 2537.
[26] Z. Zheng, J. Wang, P. Bi, J. Ren, Y. Wang, Y. Yang, X. Liu, S. Zhang, J. Hou, *Joule* **2022**, *6*, 171.
[27] P. Bi, J. Wang, Y. Cui, J. Zhang, T. Zhang, Z. Chen, J. Qiao, J. Dai, S. Zhang, X. Hao, Z. Wei, J. Hou, *Adv. Mater.* **2023**, *4*, 2210865.
[28] B. Ehrler, E. Alarcón-Lladó, S. W. Tabernig, T. Veeken, E. C. Garnett, A. Polman, *ACS Energy Lett.* **2020**, *5*, 3029.
[29] W. Shockley, H. J. Queisser, *J. Appl. Phys.* **1961**, *32*, 510.
[30] K. Vandewal, J. Benduhn, V. C. Nikolis, *Sustain. Energy Fuels* **2018**, *2*, 538.
[31] Y. Wang, D. Qian, Y. Cui, H. Zhang, J. Hou, K. Vandewal, T. Kirchartz, F. Gao, *Adv. Energy Mater.* **2018**, *8*, 1801352.
[32] U. Rau, B. Blank, T. C. M. Müller, T. Kirchartz, *Phys. Rev. Appl.* **2017**, *7*, 044016.
[33] M. A. Green, E. D. Dunlop, J. Hohl-Ebinger, M. Yoshita, N. Kopidakis, X. Hao, *Prog. Photovolt. Res. Appl.* **2022**, *30*, 3.
[34] K. Yoshikawa, H. Kawasaki, W. Yoshida, T. Irie, K. Konishi, K. Nakano, T. Uto, D. Adachi, M. Kanematsu, H. Uzu, K. Yamamoto, *Nat. Energy* **2017**, *2*, 17032.
[35] B. M. Kayes, H. Nie, R. Twist, S. G. Spruytte, F. Reinhardt, I. C. Kizilyalli, G. S. Higashi, 37th IEEE Photovolt. Spec. Conf., IEEE, 19-24 June **2011**, pp. 000004–000008.
[36] M. Nakamura, K. Yamaguchi, Y. Kimoto, Y. Yasaki, T. Kato, H. Sugimoto, *IEEE J. Photovoltaics* **2019**, *9*, 1863.
[37] M. A. Green, A. W. Y. Ho-Baillie, *ACS Energy Lett.* **2019**, *4*, 1639.
[38] M. Jeong, I. W. Choi, E. M. Go, Y. Cho, M. Kim, B. Lee, S. Jeong, Y. Jo, H. W. Choi, J. Lee, J.-H. Bae, S. K. Kwak, D. S. Kim, C. Yang, *Science* **2020**, *369*, 1615.
[39] U. Rau, *Phys. Rev. B* **2007**, *76*, 085303.
[40] L. Krückemeier, P. Kaienburg, J. Flohre, K. Bittkau, I. Zonno, B. Krogmeier, T. Kirchartz, *Commun. Phys.* **2018**, *1*, 27.
[41] D. Luo, R. Su, W. Zhang, Q. Gong, R. Zhu, *Nat. Rev. Mater.* **2019**, *5*, 44.
[42] C. M. Wolff, P. Caprioglio, M. Stolterfoht, D. Neher, *Adv. Mater.* **2019**, *31*, 1902762.
[43] A. J. Gillett, A. Privitera, R. Dilmurat, A. Karki, D. Qian, A. Pershin, G. Londi, W. K. Myers, J. Lee, J. Yuan, S.-J. Ko, M. K. Riede, F. Gao, G. C. Bazan, A. Rao, T.-Q. Nguyen, D. Beljonne, R. H. Friend, *Nature* **2021**, *597*, 666.
[44] J. V. Caspar, T. J. Meyer, *J. Phys. Chem.* **1983**, *87*, 952.
[45] A. Nitzan, S. Mukamel, J. Jortner, *J. Chem. Phys.* **1975**, *63*, 200.
[46] J. Benduhn, K. Tvingstedt, F. Piersimoni, S. Ullbrich, Y. Fan, M. Tropiano, K. A. McGarry, O. Zeika, M. K. Riede, C. J. Douglas, S. Barlow, S. R. Marder, D. Neher, D. Spoltore, K. Vandewal, *Nat. Energy* **2017**, *2*, 17053.
[47] X.-K. Chen, D. Qian, Y. Wang, T. Kirchartz, W. Tress, H. Yao, J. Yuan, M. Hülsbeck, M. Zhang, Y. Zou, Y. Sun, Y. Li, J. Hou, O. Inganäs, V. Coropceanu, J.-L. Bredas, F. Gao, *Nat. Energy* **2021**, *6*, 799.
[48] F. D. Eisner, M. Azzouzi, Z. Fei, X. Hou, T. D. Anthopoulos, T. J. S. Dennis, M. Heeney, J. Nelson, *J. Am. Chem. Soc.* **2019**, *141*, 6362.
[49] D. Qian, Z. Zheng, H. Yao, W. Tress, T. R. Hopper, S. Chen, S. Li, J. Liu, S. Chen, J. Zhang, X.-K. Liu, B. Gao, L. Ouyang, Y. Jin, G. Pozina, I. A. Buyanova, W. M. Chen, O. Inganäs, V. Coropceanu, J.-L. Bredas, H. Yan, J. Hou, F. Zhang, A. A. Bakulin, F. Gao, *Nat. Mater.* **2018**, *17*, 703.
[50] K. D. Rosenthal, M. P. Hughes, B. R. Luginbuhl, N. A. Ran, A. Karki, S. Ko, H. Hu, M. Wang, H. Ade, T. Nguyen, *Adv. Energy Mater.* **2019**, *9*, 1901077.
[51] S. Karuthedath, J. Gorenflot, Y. Firdaus, N. Chaturvedi, C. S. P. De Castro, G. T. Harrison, J. I. Khan, A. Markina, A. H. Balawi, T. A. Dela Peña, W. Liu, R.-Z. Liang, A. Sharma, S. H. K. Paleti, W. Zhang, Y. Lin, E. Alarousu, D. H. Anjum, P. M. Beaujuge, S. De Wolf, I. McCulloch, T. D. Anthopoulos, D. Baran, D. Andrienko, F. Laquai, *Nat. Mater.* **2021**, *20*, 378.
[52] Z. Tang, J. Wang, A. Melianas, Y. Wu, R. Kroon, W. Li, W. Ma, M. R. Andersson, Z. Ma, W. Cai, W. Tress, O. Inganäs, *J. Mater. Chem. A* **2018**, *6*, 12574.
[53] L. Perdigón-Toro, L. Q. Phuong, F. Eller, G. Freychet, E. Saglamkaya, J. I. Khan, Q. Wei, S. Zeiske, D. Kroh, S. Wedler, A. Köhler, A. Armin, F. Laquai, E. M. Herzig, Y. Zou, S. Shoaee, D. Neher, *Adv. Energy Mater.* **2022**, *12*, 2103422.
[54] Y. Zhang, Y. Lang, G. Li, *EcoMat* **2023**, *5*, e12281.
[55] G. Kupgan, X. K. Chen, J. L. Brédas, *Mater. Today Adv.* **2021**, *11*, 100154.
[56] Y. Ma, M. Zhang, S. Wan, P. Yin, P. Wang, D. Cai, F. Liu, Q. Zheng, *Joule* **2021**, *5*, 197.

[57] Y. Fu, T. H. Lee, Y. C. Chin, R. A. Pacalaj, C. Labanti, S. Y. Park, Y. Dong, H. W. Cho, J. Y. Kim, D. Minami, J. R. Durrant, J. S. Kim, *Nat. Commun.* **2023**, *14*, 1870.
[58] J. C. Blakesley, D. Neher, *Phys. Rev. B* **2011**, *84*, 075210.
[59] N. Jain, N. Chandrasekaran, A. Sadhanala, R. H. Friend, C. R. McNeill, D. Kabra, *J. Mater. Chem. A* **2017**, *5*, 24749.
[60] S. U. Z. Khan, J. Bertrandie, M. Gui, A. Sharma, W. Alsufyani, J. F. Gorenflot, F. Laquai, D. Baran, B. P. Rand, *Joule* **2022**, *6*, 2821.
[61] S. Xie, Y. Xia, Z. Zheng, X. Zhang, J. Yuan, H. Zhou, Y. Zhang, *Adv. Funct. Mater.* **2018**, *28*, 1705659.
[62] Q. Liu, S. Smeets, S. Mertens, Y. Xia, A. Valencia, J. D'Haen, W. Maes, K. Vandewal, *Joule* **2021**, *5*, 2365.
[63] K. Vandewal, S. Mertens, J. Benduhn, Q. Liu, *J. Phys. Chem. Lett.* **2020**, *11*, 129.
[64] K. Vandewal, S. Albrecht, E. T. Hoke, K. R. Graham, J. Widmer, J. D. Douglas, M. Schubert, W. R. Mateker, J. T. Bloking, G. F. Burkhard, A. Sellinger, J. M. J. Fréchet, A. Amassian, M. K. Riede, M. D. McGehee, D. Neher, A. Salleo, *Nat. Mater.* **2014**, *13*, 63.
[65] S. Zeiske, O. J. Sandberg, N. Zarrabi, W. Li, P. Meredith, A. Armin, *Nat. Commun.* **2021**, *12*, 3603.
[66] N. Schopp, H. M. Luong, B. R. Luginbuhl, P. Panoy, D. Choi, V. Promarak, V. V. Brus, T.-Q. Nguyen, *ACS Energy Lett.* **2022**, *7*, 1626.
[67] A. Rao, P. C. Y. Chow, S. Gélinas, C. W. Schlenker, C.-Z. Li, H.-L. Yip, A. K. Y. Jen, D. S. Ginger, R. H. Friend, *Nature* **2013**, *500*, 435.
[68] Z. Chen, X. Chen, Z. Jia, G. Zhou, J. Xu, Y. Wu, X. Xia, X. Li, X. Zhang, C. Deng, Y. Zhang, X. Lu, W. Liu, C. Zhang, Y. (Michael) Yang, H. Zhu, *Joule* **2021**, *5*, 1832.
[69] O. J. Sandberg, A. Armin, *J. Phys. Chem. C* **2021**, *125*, 15590.
[70] T. M. Burke, S. Sweetnam, K. Vandewal, M. D. McGehee, *Adv. Energy Mater.* **2015**, *5*, 1500123.
[71] M. Azzouzi, J. Yan, T. Kirchartz, K. Liu, J. Wang, H. Wu, J. Nelson, *Phys. Rev. X* **2018**, *8*, 031055.
[72] S. Ullbrich, J. Benduhn, X. Jia, V. C. Nikolis, K. Tvingstedt, F. Piersimoni, S. Roland, Y. Liu, J. Wu, A. Fischer, D. Neher, S. Reineke, D. Spoltore, K. Vandewal, *Nat. Mater.* **2019**, *18*, 459.
[73] Y. Xu, Y. Cui, H. Yao, T. Zhang, J. Zhang, L. Ma, J. Wang, Z. Wei, J. Hou, *Adv. Mater.* **2021**, *33*, 2101090.
[74] G.-J. A. H. Wetzelaer, M. Scheepers, A. M. Sempere, C. Momblona, J. Ávila, H. J. Bolink, *Adv. Mater.* **2015**, *27*, 1837.
[75] A. Karki, J. Vollbrecht, A. L. Dixon, N. Schopp, M. Schrock, G. N. M. Reddy, T. Nguyen, *Adv. Mater.* **2019**, *31*, 1903868.
[76] J. Hofinger, S. Weber, F. Mayr, A. Jodlbauer, M. Reinfelds, T. Rath, G. Trimmel, M. C. Scharber, *J. Mater. Chem. A* **2022**, *10*, 2888.
[77] N. An, Y. Cai, H. Wu, A. Tang, K. Zhang, X. Hao, Z. Ma, Q. Guo, H. S. Ryu, H. Y. Woo, Y. Sun, E. Zhou, *Adv. Mater.* **2020**, *32*, 2002122.
[78] P. Bi, S. Zhang, J. Ren, Z. Chen, Z. Zheng, Y. Cui, J. Wang, S. Wang, T. Zhang, J. Li, Y. Xu, J. Qin, C. An, W. Ma, X. Hao, J. Hou, *Adv. Mater.* **2022**, *34*, 2108090.
[79] J. Wang, L. Ma, Y. W. Lee, H. Yao, Y. Xu, S. Zhang, H. Y. Woo, J. Hou, *Chem. Commun.* **2021**, *57*, 9132.
[80] B. Gao, H. Yao, L. Hong, J. Hou, *Chin. J. Chem.* **2019**, *37*, 1153.
[81] A. Jungbluth, P. Kaienburg, M. Riede, *J. Phys. Mater.* **2022**, *5*, 024002.
[82] D. Abou-Ras, T. Kirchartz, U. Rau, in *Advanced Characterization Techniques for Thin Film Solar Cells*, Wiley, New Jersey, USA **2011**.
[83] K. Vandewal, K. Tvingstedt, A. Gadisa, O. Inganäs, J. V. Manca, *Nat. Mater.* **2009**, *8*, 904.
[84] L. Krückemeier, U. Rau, M. Stolterfoht, T. Kirchartz, *Adv. Energy Mater.* **2020**, *10*, 1902573.
[85] H. Lu, W. Liu, H. Jin, H. Huang, Z. Tang, Z. Bo, *Adv. Funct. Mater.* **2022**, *32*, 2107756.
[86] A. Zampetti, A. Minotto, F. Cacialli, *Adv. Funct. Mater.* **2019**, *29*, 1807623.
[87] M. Vasilopoulou, A. Fakharuddin, F. P. García de Arquer, D. G. Georgiadou, H. Kim, A. R. bin Mohd Yusoff, F. Gao, M. K. Nazeeruddin, H. J. Bolink, E. H. Sargent, *Nat. Photon.* **2021**, *15*, 656.
[88] R. Wang, J. Xu, L. Fu, C. Zhang, Q. Li, J. Yao, X. Li, C. Sun, Z.-G. Zhang, X. Wang, Y. Li, J. Ma, M. Xiao, *J. Am. Chem. Soc.* **2021**, *143*, 4359.
[89] J. M. Marin-Beloqui, D. T. W. Toolan, N. A. Panjwani, S. Limbu, J. Kim, T. M. Clarke, *Adv. Energy Mater.* **2021**, *11*, 2100539.
[90] Y. Xu, H. Yao, L. Ma, L. Hong, J. Li, Q. Liao, Y. Zu, J. Wang, M. Gao, L. Ye, J. Hou, *Angew. Chem., Int. Ed.* **2020**, *59*, 9004.
[91] J. Zhang, W. Liu, M. Zhang, Y. Liu, G. Zhou, S. Xu, F. Zhang, H. Zhu, F. Liu, X. Zhu, *iScience* **2019**, *19*, 883.
[92] Z. Zheng, M. Li, Z. Qin, E. He, Y. Yin, F. Guo, S. Gao, X. Pang, L. Zhao, Z. Tang, X. Lu, Y. Zhang, *J. Mater. Chem. A* **2021**, *9*, 15798.
[93] L. Ye, K. Weng, J. Xu, X. Du, S. Chandrabose, K. Chen, J. Zhou, G. Han, S. Tan, Z. Xie, Y. Yi, N. Li, F. Liu, J. M. Hodgkiss, C. J. Brabec, Y. Sun, *Nat. Commun.* **2020**, *11*, 6005.
[94] Y. Zhang, L. Pan, Z. Peng, W. Deng, B. Zhang, X. Yuan, Z. Chen, L. Ye, H. Wu, X. Gao, Z. Liu, C. Duan, F. Huang, Y. Cao, *J. Mater. Chem. A* **2021**, *9*, 13522.
[95] J. Liang, M. Pan, G. Chai, Z. Peng, J. Zhang, S. Luo, Q. Han, Y. Chen, A. Shang, F. Bai, Y. Xu, H. Yu, J. Y. L. Lai, Q. Chen, M. Zhang, H. Ade, H. Yan, *Adv. Mater.* **2020**, *32*, 2003500.
[96] X. Yuan, Y. Zhao, D. Xie, L. Pan, X. Liu, C. Duan, F. Huang, Y. Cao, *Joule* **2022**, *6*, 647.
[97] J. Wu, G. Li, J. Fang, X. Guo, L. Zhu, B. Guo, Y. Wang, G. Zhang, L. Arunagiri, F. Liu, H. Yan, M. Zhang, Y. Li, *Nat. Commun.* **2020**,*11*, 4612.
[98] J. Wang, X. Jiang, H. Wu, G. Feng, H. Wu, J. Li, Y. Yi, X. Feng, Z. Ma, W. Li, K. Vandewal, Z. Tang, *Nat. Commun.* **2021**, *12*, 6679.
[99] Y. Shi, Y. Chang, K. Lu, Z. Chen, J. Zhang, Y. Yan, D. Qiu, Y. Liu, M. A. Adil, W. Ma, X. Hao, L. Zhu, Z. Wei, *Nat. Commun.* **2022**, *13*, 3256.
[100] V. Coropceanu, X.-K. Chen, T. Wang, Z. Zheng, J.-L. Brédas, *Nat. Rev. Mater.* **2019**, *4*, 689.
[101] Z.-H. Chen, P.-Q. Bi, X.-Y. Yang, M.-S. Niu, K.-N. Zhang, L. Feng, X.-T. Hao, *J. Phys. Chem. C* **2019**, *123*, 12676.
[102] Q. He, W. Sheng, M. Zhang, G. Xu, P. Zhu, H. Zhang, Z. Yao, F. Gao, F. Liu, X. Liao, Y. Chen, *Adv. Energy Mater.* **2021**, *11*, 2003390.
[103] K. Zhang, J. Liu, Y. Zhang, J. Fan, C.-K. Wang, L. Lin, *J. Phys. Chem. C* **2019**, *123*, 24705.
[104] H. Cha, G. Fish, J. Luke, A. Alraddadi, H. H. Lee, W. Zhang, Y. Dong, S. Limbu, A. Wadsworth, I. P. Maria, L. Francàs, H. L. Sou, T. Du, J. Kim, M. A. McLachlan, I. McCulloch, J. R. Durrant, *Adv. Energy Mater.* **2019**, *9*, 1901254.
[105] R. Yu, H. Yao, Y. Cui, L. Hong, C. He, J. Hou, *Adv. Mater.* **2019**, *31*, 1902302.
[106] L. Zuo, S. B. Jo, Y. Li, Y. Meng, R. J. Stoddard, Y. Liu, F. Lin, X. Shi, F. Liu, H. W. Hillhouse, D. S. Ginger, H. Chen, A. K. Y. Jen, *Nat. Nanotechnol.* **2022**, *17*, 53.
[107] C. He, Y. Li, Y. Liu, Y. Li, G. Zhou, S. Li, H. Zhu, X. Lu, F. Zhang, C.-Z. Li, H. Chen, *J. Mater. Chem. A* **2020**, *8*, 18154.
[108] Z. Zhang, Y. Li, G. Cai, Y. Zhang, X. Lu, Y. Lin, *J. Am. Chem. Soc.* **2020**, *142*, 18741.
[109] Z. Huang, Y. Shi, Y. Chang, C. Yang, M. Lv, Y. Shen, Y. Liu, J. Zhang, K. Lu, Z. Wei, *J. Mater. Chem. C* **2022**, *10*, 2800.
[110] A. M. Kay, O. J. Sandberg, N. Zarrabi, W. Li, S. Zeiske, C. Kaiser, P. Meredith, A. Armin, *Adv. Funct. Mater.* **2022**, *32*, 2113181.
[111] V. C. Nikolis, A. Mischok, B. Siegmund, J. Kublitski, X. Jia, J. Benduhn, U. Hörmann, D. Neher, M. C. Gather, D. Spoltore, K. Vandewal, *Nat. Commun.* **2019**, *10*, 3706.
[112] Q. Liu, J. Toudert, T. Li, M. Kramarenko, G. Martínez-Denegri, L. Ciammaruchi, X. Zhan, J. Martorell, *Adv. Energy Mater.* **2019**, *9*, 1900463.

[113] C. Kaiser, O. J. Sandberg, N. Zarrabi, W. Li, P. Meredith, A. Armin, *Nat. Commun.* **2021**, *12*, 3988.
[114] J. Yan, E. Rezasoltani, M. Azzouzi, F. Eisner, J. Nelson, *Nat. Commun.* **2021**, *12*, 3642.
[115] N. A. Ran, S. Roland, J. A. Love, V. Savikhin, C. J. Takacs, Y.-T. Fu, H. Li, V. Coropceanu, X. Liu, J.-L. Brédas, G. C. Bazan, M. F. Toney, D.i. Neher, T.-Q. Nguyen, *Nat. Commun.* **2017**, *8*, 79.
[116] L. Yang, S. Zhang, C. He, J. Zhang, Y. Yang, J. Zhu, Y. Cui, W. Zhao, H. Zhang, Y. Zhang, Z. Wei, J. Hou, *Chem. Mater.* **2018**, *30*, 2129.
[117] K. Zhou, Y. Wu, Y. Liu, X. Zhou, L. Zhang, W. Ma, *ACS Energy Lett.* **2019**, *4*, 1057.
[118] L. Wang, S. Guo, K. Zhou, W. Ma, *Sustain. Energy Fuels* **2020**, *4*, 4934.
[119] C. Yang, J. Zhang, N. Liang, H. Yao, Z. Wei, C. He, X. Yuan, J. Hou, *J. Mater. Chem. A* **2019**, *7*, 18889.
[120] J. Liu, S. Chen, D. Qian, B. Gautam, G. Yang, J. Zhao, J. Bergqvist, F. Zhang, W. Ma, H. Ade, O. Inganäs, K. Gundogdu, F. Gao, H. Yan, *Nat. Energy* **2016**, *1*, 16089.
[121] J. Bertrandie, J. Han, C. S. P. De Castro, E. Yengel, J. Gorenflot, T. Anthopoulos, F. Laquai, A. Sharma, D. Baran, *Adv. Mater.* **2022**, *34*, 2202575.
[122] A. Classen, C. L. Chochos, L. Lüer, V. G. Gregoriou, J. Wortmann, A. Osvet, K. Forberich, I. McCulloch, T. Heumüller, C. J. Brabec, *Nat. Energy* **2020**, *5*, 711.
[123] Y. Xie, H. Wu, *Mater. Today Adv.* **2020**, *5*, 100048.
[124] Y. Xie, W. Wang, W. Huang, F. Lin, T. Li, S. Liu, X. Zhan, Y. Liang, C. Gao, H. Wu, Y. Cao, *Energy Environ. Sci.* **2019**, *12*, 3556.
[125] Y. Dong, H. Cha, H. L. Bristow, J. Lee, A. Kumar, P. S. Tuladhar, I. McCulloch, A. A. Bakulin, J. R. Durrant, *J. Am. Chem. Soc.* **2021**, *143*, 7599.
[126] T. F. Hinrichsen, C. C. S. Chan, C. Ma, D. Paleček, A. Gillett, S. Chen, X. Zou, G. Zhang, H.-L. Yip, K. S. Wong, R. H. Friend, H. Yan, A. Rao, P. C. Y. Chow, *Nat. Commun.* **2020**, *11*, 5617.
[127] H. Wu, Z. Ma, M. Li, H. Lu, A. Tang, E. Zhou, J. Wen, Y. Sun, W. Tress, J. M. H. Olsen, S. Meloni, Z. Bo, Z. Tang, *Energy Environ. Sci.* **2023**, *16*, 1277.

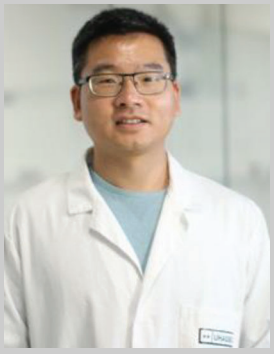

Quan Liu received his Ph.D. degree in photonics engineering through an Erasmus Mundus Joint Doctorate program from Polytechnic University of Catalonia (UPC, Barcelona) and Karlsruhe Institute of Technology (KIT, Karlsruhe) in 2018. He centered his doctoral work on photon management in organic photovoltaics. Afterward, he spent 1 year as postdoctoral fellow at ICFO (Spain) and another approximately 4 years at Hasselt University (Belgium). During the period of 2020–2022, he was funded by Marie–Curie postdoctoral fellowship action (MSCA). In January 2023, he moved to NIMTE of Chinese Academy of Sciences as a professor, working on organic transparent photovoltaics and near-infrared photodetectors.

Koen Vandewal obtained his Ph.D. in physics at Hasselt University in 2009 working on the physics of organic photovoltaics. After that, he spent 2 years as a postdoctoral fellow at Linköping University in Sweden and another 2 years at Stanford University (USA). In 2014, he was appointed as endowed professor at the Technische Universität (TU) Dresden in Germany. In January 2018, he moved from TU Dresden to Hasselt University, leading a research group with the aim to solve fundamental questions in the field of organic, hybrid, and molecular electronics with relevance to applications in electronic devices.